A Numerical Investigation of Mixed-Layer Dynamics

PIJUSH K. KUNDU

Ocean Sciences Center, Nova University, Dania, FL 33004

(Manuscript received 6 April 1979, in final form 5 September)

ABSTRACT

The structure of the stratified turbulent upper mixed layer of the ocean has been numerically investigated by using the turbulence closure model of Gibson and Launder, under the action of an impulsive wind stress τ_0 and zero surface heat flux. The values of buoyancy and Coriolis frequencies assumed are $N = 0.94 \times 10^{-2}$ s^{-1} and $f = 10^{-4}$ s^{-1}, respectively. The solutions indicate that the turbulent diffusion terms, small in general, transfer kinetic energy downward, although its effect on the deepening is negligible. Let t_i be the time in inertial periods and u_* be the friction velocity. Then for $0.05 < t_i < 0.3$, the rate of increase of potential energy in the water column varies as $\partial(\text{PE})/\partial t \propto t^{1/2}$, rising to a maximum of $\sim 1.1 u_*^3$ and implying a mixed layer depth $h \propto t^{1/2}$ as in the Pollard-Rhines-Thompson (PRT) model. For $1 < t_i < 6$, $\partial(\text{PE})/\partial t$ decreases only slightly from a quasi-steady value of $\partial(\text{PE})/\partial t \approx 0.25 u_*^3$, implying a deepening rate slightly smaller than the Kraus-Turner $h \propto t^{1/3}$. The reason for this difference in behavior for the two time ranges is the separation of the flow into a depth-independent inertial oscillation and a quasi-steady shearing flow that carries almost all the turbulent stresses in the water column. The mechanism for deepening is always the lifting of heavier mass by the locally generated turbulence at the base of the mixed layer. For very large times ($t_i > 12$), $\partial(\text{PE})/\partial t$ drops sharply, and no deepening was detected with a vertical resolution of 1 m. The assumption necessary to derive the PRT energy equation, namely, that the depth-integrated dissipation nearly balances $\tau_0 \cdot (U_0 - \hat{U})$, where U_0 is the surface velocity and $\hat{U}$ the depth-averaged velocity, is approximately valid. For $t_i < 0.25$, the PRT bulk Richardson number criterion is equivalent to a local critical gradient Richardson number criterion, and is due to the self-similarity of the solutions and the consequent thickening of the "interface." The self-similarity breaks down for larger times, either because of the Coriolis forces becoming more important or because of the appearance of a sharp interface due to a nonlinear mechanism, whichever is earlier. An imposition of a kinetic energy input at the sea surface, so as to simulate the wind-wave flux, has certain desirable features.

1. Introduction

The dynamics of the upper surface layer of the ocean has received a great deal of attention recently, because it is in this layer that the ocean exchanges heat and momentum with the atmosphere. The basic theoretical works in this area are those of Kraus and Turner (1967) and Pollard *et al.* (1973, hereafter referred to as PRT). The Kraus-Turner model does not consider mean velocities, but equates the rate of turbulent kinetic energy produced by wind waves with the rate of increase of potential energy due to deepening. This implies that the wind-wave production of turbulent kinetic energy is diffused downward, and is used in lifting the heavier mass from below the mixed-layer base. The PRT model, on the other hand, equates the rate of work done by the wind stress on the mean motion, which in their case is a depth-independent inertial oscillation, to the rate of increase of kinetic and potential energies of the mean field. Niiler (1975) showed that the PRT mean energetics is equivalent to equating the potential energy increase to the shear production by the entrainment stress at the mixed-layer base. He and de Szoeke and Rhines (1976) showed that the Kraus-Turner and PRT models are two asymptotic limits of the general balance of the turbulent kinetic energy equation.

The theoretical bulk models do not give vertical distributions of variables so that they could be compared with the observations. The assumption of no velocity shear in the upper layer does not agree with most of the observations. For example, Halpern (1976), Gonella (1970), Pollard (1972 JASIN data, unpublished) and Davis (1978 MILE data, unpublished) all observed mean shears of the order 10^{-2} s^{-1}, which is somewhat larger than the buoyancy frequency N. In particular, Halpern's surface layer data (Halpern, 1976; Kundu, 1976) displayed intriguing Ekman spirals for sub-inertial time scale motions.

As Phillips (1977, p. 303) notes, numerical models are necessary in order to determine more realistic distributions of velocity, temperature, turbulence intensity, dissipation, etc. Such models make the so-called second-order turbulence closure assumptions, and relate the turbulent stresses with the mean field. The first such numerical model of the oceanic mixed

0022-3670/80/020220-17$08.25

layer was by Mellor and Durbin (1975). They neglected the vertical diffusion of turbulent kinetic energy, and assumed that the local rate of its generation is balanced by the local rate of dissipation. They were then able to write explicit algebraic expressions for the turbulent stresses, kinetic energy, dissipation, etc., and obtained several interesting solutions for a variety of boundary conditions.

An important question is whether or not the turbulent diffusion is really negligible everywhere, as Mellor and Durbin assumed. Order-of-magnitude considerations may be misleading, since sharp changes can appear across the interface. It is important to resolve this question, since the Kraus-Turner model in contrast implies that all of the wind-generated turbulence near the surface is diffused downward and is used for increasing the potential energy due to deepening. The model of Garwood (1977), and that of Tennekes (1973) for convective atmospheric boundary layers, also assume that the balance at the mixed-layer base is between the turbulent diffusion and the buoyant damping.

In order to investigate the importance of turbulent diffusion, we decided to model the turbulence according to that of Gibson and Launder (1976), where such terms are retained. Most applications to geophysical turbulent flow problems use the models of either Lumley and his co-workers (e.g., Wyngaard *et al.*, 1974; Zeman and Lumley, 1976), or Mellor and his co-workers (e.g., Mellor and Durbin, 1975; Worthem and Mellor, 1980). The models of Launder and his co-workers, on the other hand, have been extensively tested against laboratory flows, but have never been applied in geophysical conditions. In the present work, it was decided to use the turbulence model of Gibson and Launder (1976), because it considers gravitational effects (and is therefore applicable to a stratified field), retains the turbulent diffusion terms, and is yet simpler than models that solve differential equations for all components of the Reynolds fluxes. A somewhat similar model has also been used by Worthem and Mellor (1980) to study tropical upper ocean.

For the case of the stable mixed layer driven by a wind stress with no heat flux on top, it will be shown (Fig. 8) that if a zero flux of q^2 is assumed at the ocean surface $z = 0$, then the diffusion term is especially small near the interface, although it can be as large as the local rate of change of potential energy in most parts. However, the zero q^2 flux condition at $z = 0$ may be unrealistic, since the breaking of wind waves would create an effective flux of q^2 at the upper surface. Some preliminary results have therefore been obtained with a kinetic energy flux at the surface to simulate the breaking waves. It will be shown that the introduction of this surface flux produces some desirable features in the solutions but its contribution to mixed-layer deepening is negligible.

Another important objective of the present study is to compare the present numerical calculations with the theoretical predictions of the Kraus-Turner and PRT models. A critical quantity for this discussion is the behavior with time of the rate of change of potential energy in the water column, $\partial(\mathrm{PE})/\partial t$ (Fig. 6). It will be shown that for times smaller than about quarter of an inertial period $\partial(\mathrm{PE})/\partial t \propto t^{1/2}$, implying a mixed layer depth $h \propto t^{1/2}$ as in the PRT model. It is shown here, as well as in Kundu (1980), that for this time range the solutions develop in a self-similar manner, and the bulk Richardson number criterion of PRT has physical validity since it is equivalent to a critical gradient Richardson number criterion at the base of the mixed layer. On the other hand, for times larger than an inertial period, $\partial(\mathrm{PE})/\partial t$ decreases very slowly from a quasi-steady value, implying a deepening rate only slightly slower than the Kraus-Turner $h \propto t^{1/3}$.

To summarize the objectives of the present work are to 1) investigate the importance of turbulent diffusion, both with and without surface flux of kinetic energy; 2) generate vertical profiles of quantities that could be measured in the real ocean, for example, dissipation, Reynolds stresses, length scales of large eddies, eddy diffusivities, mean velocity and temperature, etc.; and 3) compare solutions with the principal theoretical works on oceanic mixed layers.

2. The model

a. Equations of motion and the turbulent fluxes

The present model, like all the others quoted so far, is one-dimensional in nature in that horizontal variations are neglected. Due to insufficient observations, it is not clear how good this assumption is. Denman and Miyake (1973) concluded that horizontal advection is not significant in the heat budget for periods less than several weeks, and Niiler and Kraus (1977) also argued that these effects are small. Price *et al.* (1978), on the other hand, suggested that the advective effects are important, although not overwhelming. In any case, a one-dimensional model will be used here because it is simple, and yet sufficiently comprehensive to answer the questions addressed in the Introduction.

The equations of mean motion are

$$\left.\begin{aligned} \frac{\partial U}{\partial t} - fV &= \frac{\partial}{\partial z}\left(-\overline{uw} + \nu\frac{\partial U}{\partial z}\right) \\ \frac{\partial V}{\partial t} + fU &= \frac{\partial}{\partial z}\left(-\overline{vw} + \nu\frac{\partial V}{\partial z}\right) \\ \frac{\partial T}{\partial t} &= \frac{\partial}{\partial z}\left(-\overline{\theta w} + k\frac{\partial T}{\partial z}\right) \end{aligned}\right\}, \qquad (1)$$

where (u,v,w) are turbulent velocity components in the (x,y,z) directions, z is positive upward, (U,V) are mean horizontal velocity components, θ is the fluctuating temperature, T the mean temperature, f the Coriolis parameter, and ν and k the molecular diffusivities of momentum and heat, respectively.

The turbulent fluxes in Eq. (1) are modeled here according to the proposal of Gibson and Launder. Only an outline of this model is presented here. The original work should be consulted for further details.

In Cartesian tensor notation, the model equations for the determination of Reynolds stresses $-\overline{u_iu_j}$ are (Launder, 1975)

$$\frac{D\overline{u_iu_j}}{Dt} = -\frac{\partial}{\partial x_k}(\overline{u_iu_ju_k}) + P_{ij} - \tfrac{2}{3}\delta_{ij}\epsilon$$

diffusive transport; pro- duction; viscous dissipation

$$- 2.2\frac{\epsilon}{q^2}(\overline{u_iu_j} - \tfrac{2}{3}\delta_{ij}q^2) - 0.55(P_{ij} - \tfrac{2}{3}\delta_{ij}P), \quad (2)$$

pressure scrambling

where

$$P_{ij} = -\left(\overline{u_iu_k}\frac{\partial U_j}{\partial x_k} + \overline{u_ju_k}\frac{\partial U_i}{\partial x_k}\right) - \beta(g_j\overline{u_i\theta} + g_i\overline{u_j\theta}),$$

$$P = -\overline{u_iu_k}\frac{\partial U_i}{\partial x_k} - \beta g_i\overline{u_i\theta} = \tfrac{1}{2}P_{ii},$$

$$q^2 = \tfrac{1}{2}\overline{u_iu_i}.$$

Here i and j can be 1, 2 or 3; δ_{ij} is the Kronecker delta, P and ϵ are, respectively, the rates of production and viscous dissipation of turbulent kinetic energy q^2, β is the coefficient of thermal expansion, and $\mathbf{g} = (0,0,-g)$ is the gravitational vector. The "pressure scrambling" term $\overline{p(\partial u_i/\partial x_j + \partial u_j/\partial x_i)}$ is modelled by the last two terms in Eq. (2). Setting $i = j$, and summing gives an equation for turbulent kinetic energy:

$$\frac{Dq^2}{Dt} = -\frac{\partial}{\partial x_k}(\overline{q^2u_k}) + P - \epsilon. \quad (2')$$

Eq. (2), along with similar equations for $\overline{u_i\theta}$ and ϵ, can be solved for the turbulent fluxes. Simple algebraic equations for $\overline{u_iu_j}$ would result if the left-hand side and the diffusive transport terms are altogether neglected in Eq. (2), as was done by Mellor and Durbin. However, another way to achieve the same effect is to assume that (Rodi, 1972)

$$\frac{D\overline{u_iu_j}}{Dt} + \frac{\partial}{\partial x_k}(\overline{u_iu_ju_k}) = \frac{\overline{u_iu_j}}{q^2}\left[\frac{Dq^2}{Dt} + \frac{\partial}{\partial x_k}(\overline{q^2u_k})\right]. \quad (3)$$

That is, the advective minus the diffusive transport of $\overline{u_iu_j}$ is locally proportional to the same for q^2, the factor of proportionality being $\overline{u_iu_j}/q^2$. According to Gibson and Launder, this is a good approximation in thin shear flows, such as the mixed layer. On using Eq. (2'), assumption (3) implies

$$\frac{D\overline{u_iu_j}}{Dt} + \frac{\partial}{\partial x_k}(\overline{u_iu_ju_k}) = \frac{\overline{u_iu_j}}{q^2}(P - \epsilon).$$

Substitution of the above into Eq. (2) now gives algebraic equations for $\overline{u_iu_j}$, which is a considerable simplification.

Treating the equation for $D(\overline{u_i\theta})/Dt$ in a similar way, and making additional assumptions about the temperature variance $\overline{\theta^2}$ and temperature dissipation ϵ_θ, the final equations of the Gibson-Launder model for a (z,t) dependent model reduce to

$$\left.\begin{aligned}
-\overline{uw} &= \frac{q^2}{\epsilon}\phi\left[\overline{w^2}\frac{\partial U}{\partial z} - \beta g\overline{u\theta}\right]\\
-\overline{vw} &= \frac{q^2}{\epsilon}\phi\left[\overline{w^2}\frac{\partial V}{\partial z} - \beta g\overline{v\theta}\right]\\
\overline{w^2} &= \frac{2q^2}{3}\left(1 - \frac{P}{\epsilon}\phi\right) - 2q^2\frac{P}{\epsilon}\phi\frac{R_f}{1 - R_f}\\
-\overline{u\theta} &= \phi_T\frac{q^2}{\epsilon}\overline{uw}\frac{\partial T}{\partial z} + 0.5\phi_T\frac{q^2}{\epsilon}\overline{w\theta}\frac{\partial U}{\partial z}\\
-\overline{v\theta} &= \phi_T\frac{q^2}{\epsilon}\overline{vw}\frac{\partial T}{\partial z} + 0.5\phi_T\frac{q^2}{\epsilon}\overline{w\theta}\frac{\partial V}{\partial z}\\
-\overline{w\theta} &= \phi_T\frac{q^2}{\epsilon}\overline{w^2}\frac{\partial T}{\partial z} + 0.8\phi_T\frac{q^4}{\epsilon^2}\beta g\overline{w\theta}\frac{\partial T}{\partial z}
\end{aligned}\right\}, \quad (4)$$

where

$$R_f = \beta g\overline{w\theta}\left[\overline{uw}\frac{\partial U}{\partial z} + \overline{vw}\frac{\partial V}{\partial z}\right]^{-1}$$

= flux Richardson number,

$$\phi = 0.45/(1.2 + P/\epsilon),$$

$$\phi_T = [3.2 + 0.5(P/\epsilon - 1)]^{-1},$$

$$P = -\overline{uw}\frac{\partial U}{\partial z} - \overline{vw}\frac{\partial V}{\partial z} + \beta g\overline{w\theta} = P_s + \beta g\overline{w\theta}.$$

Here P_s is the shear production. The values of the numerical constants have been estimated in this model from measurements in laboratory flows. The kinetic energy and dissipation are determined by solving

$$\frac{\partial q^2}{\partial t} = \frac{\partial}{\partial z}\left(\nu_t\frac{\partial q^2}{\partial z}\right) + P - \epsilon, \quad (5)$$

$$\frac{\partial \epsilon}{\partial t} = \frac{\partial}{\partial z}\left(\frac{\nu_t}{1.3}\frac{\partial \epsilon}{\partial z}\right) + 1.45\frac{P_s\epsilon}{q^2} - 1.9\frac{\epsilon^2}{q^2}, \quad (6)$$

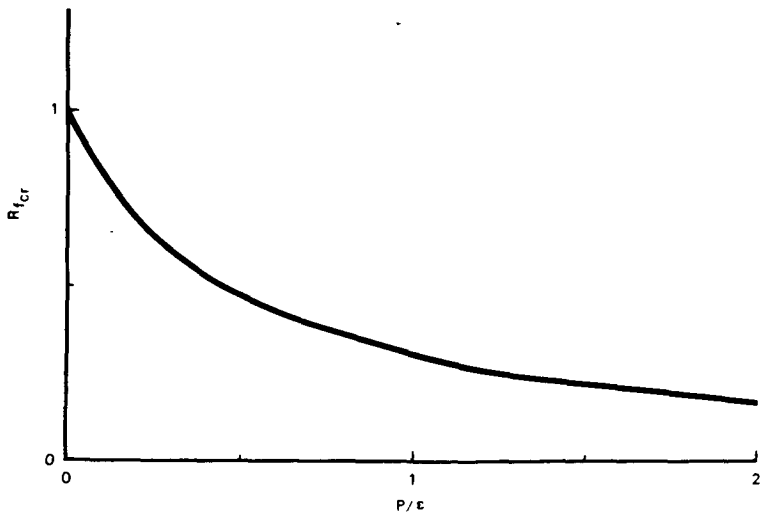

FIG. 1. Dependence of the critical Richardson number on P/ϵ according to the Gibson-Launder model.

where $\partial/\partial t$ is used instead of D/Dt because of the absence of advection in the present one-dimensional model. Eq. (5) is derived from Eq. (2') by assuming gradient diffusion $-\overline{wq^2} = \nu_t \partial q^2/\partial z$. Derivation of Eq. (6) is shown in Hanjalic and Launder (1972).

It is easy to show that if the shear stresses in (4) are written as $-\overline{uw} = \nu_t(\partial U/\partial z)$ and $-\overline{vw} = \nu_t(\partial V/\partial z)$, then the eddy viscosity is

$$\nu_t = \frac{\frac{2}{3}\phi\left(1 - \frac{P\phi}{\epsilon}\right) - 2\frac{P}{\epsilon}\phi^2\frac{R_f}{1 - R_f}}{1 + \phi\phi_T(1 + 0.5/\sigma)B}\frac{q^4}{\epsilon}, \quad (7)$$

where $B = \beta g(q^4/\epsilon^2)(\partial T/\partial z)$, and σ is the turbulent Prandtl number given by

$$\sigma = \frac{\phi}{\phi_T}\frac{1 + 0.5\phi_T(1.6 - \phi_T)B}{1 + \phi\phi_T B}.$$

The Gibson-Launder model thus consists of Eqs. (4), (5), (6) and (7), along with the mean flow equations (1). Thus, differential equations will have to be solved for U, V, T, q^2 and ϵ, along with algebraic equations for the Reynolds fluxes.

It can be shown from Eq. (7) that the eddy viscosity, and therefore the turbulent fluxes, in this model go to zero if $R_f > R_{f_{cr}}$ where

$$R_{f_{cr}} = \frac{1 + 0.46P/\epsilon}{1 + 2.78P/\epsilon + (P/\epsilon)^2}. \quad (8)$$

A plot of $R_{f_{cr}}$ against P/ϵ is given in Fig. 1 (see also Fig. 6 of Gibson and Launder). Notice that $R_{f_{cr}} \approx 0.3$ if $P/\epsilon = 1$, which is close to the value of $R_{f_{cr}} = 0.21$ in the Mellor-Durbin model.

b. Boundary and initial conditions

The initial condition was one of no motion, with a temperature distribution linearly varying from 9°C at $z = 0$ to 5°C at $z = -100$ m, which corresponds approximately to the temperature distribution across the seasonal thermocline in Fig. 1 of Denman and Miyake (1973), and gives a buoyancy frequency of $N^2 = 0.88 \times 10^{-4}$ s^{-2}. [Note that this value of N^2 is very near that assumed by Mellor and Durbin, but somewhat smaller than the value of $N^2 = 2 \times 10^{-4}$ s^{-2} used in calculations of PRT, Niiler and Kraus (1977) and Price *et al.* (1978).

The boundary conditions used are as follows:

$$z = 0: \quad \nu_t\frac{\partial U}{\partial z} = \tau_0, \quad \frac{\partial V}{\partial z} = 0, \quad \frac{\partial T}{\partial z} = 0 \qquad \text{on (1)}$$

$$\nu_t\frac{\partial q^2}{\partial z} = 0 \text{ or } F \qquad \text{on (5)}$$

$$\epsilon = P - \frac{\partial}{\partial z}\left(\nu_t\frac{\partial q^2}{\partial z}\right). \qquad \text{on (6)}$$

$$z = -100 \text{ m}: \quad U = V = 0, \quad T = \text{constant} \qquad \text{on (1)}$$

$$q^2 = 0 \qquad \text{on (5)}$$

$$\epsilon = 0. \qquad \text{on (6)}$$

The conditions on (1) are equivalent to a wind stress τ_0 in the x direction suddenly applied at $t = 0$, and a zero surface heat flux. The values of τ_0 used were 1.0, 1.5 and 2.0 dyn cm^{-2}, but the dimensional results given here all correspond to $\tau_0 = 1.5$ dyn cm^{-2}.

The surface boundary condition on Eq. (5) depends on whether one assumes a downward flux of kinetic energy F imparted at the ocean surface,

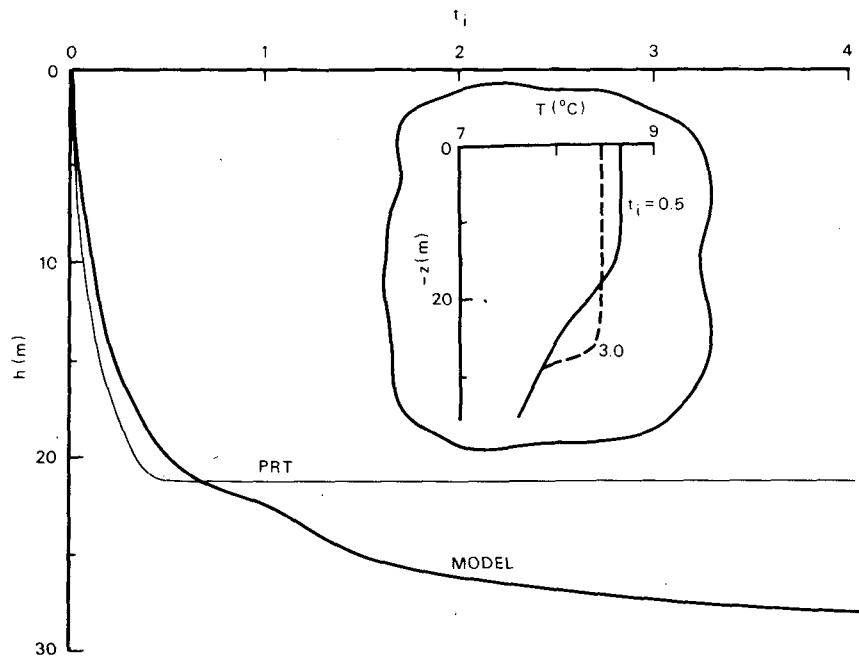

FIG. 2. Variation of the depth of the turbulent layer according to the present model and the PRT model. t_i is time in inertial periods. The inset shows the temperature profiles at two times. Wind stress τ_0 = 1.5 dyn cm^{-2}.

presumably due to the wave-wind action. The wind-wave flux F should only depend on the stress and the density of water ρ, so $F = mu_*^3$, where $u_* = (\tau_0/\rho)^{1/2}$ and m is a constant. The solutions presented here have $m = 0$ or 0.5.

The surface boundary condition on the dissipation equation (6) was obtained by setting $\partial q^2/\partial t = 0$ at $z = 0$ in (5), which is a reasonable assumption since the $\partial q^2/\partial t$ term is several orders of magnitude smaller than the other terms in Eq. (5). P was evaluated at the previous time step in this boundary condition. [In the meteorological situation one generally applies a condition like $\epsilon = u_*^3/\kappa z$ or $d\epsilon/dz = -\epsilon/z$ at the edge of a surface layer (κ = von Kármán constant), but it is unrealistic to expect a surface layer in the oceanic situation.]

The lower boundary conditions could be applied at any depth below the maximum mixed-layer depth; we chose to apply them at $z = -100$ m.

The numerical values used were $\beta g = 0.22$ cm s^2 K^{-1}, and $f = 10^{-4}$ s^{-1} corresponding to an inertial period of $T_i = 2\pi/f = 17.5$ h. Molecular values of the diffusion coefficients were used below the mixed layer, with $\nu = 0.0134$ cm^2 s^{-1} and $k = 0.00134$ cm^2 s^{-1}.

c. *Method of solution*

The set of equations (1), (5) and (6) were integrated forward in time, modeling the turbulent fluxes by (4) and using (8) to determine whether the flow was turbulent or not. The time step was $\Delta t = 60$ s, and the grid spacing was $\Delta z = 1$ m. The fluxes of heat and momentum, dissipation, and kinetic energy were defined midway between the grid points for the mean velocity and temperature, resulting in an accurate differencing procedure. An implicit scheme was used for rendering the diffusive terms stable, and standard tri-diagonal matrix routines were used for solving the resulting equations. In addition to applying a surface wind stress, a small value of ϵ was introduced at the first grid point below the surface so as to start the calculations; the resulting solutions were observed to be independent of the assumed starting value within a few time steps.

3. Results with no wave flux

Solutions will now be presented for the case where no turbulent energy flux was imposed on the sea surface; i.e., where all the turbulence was generated internally by shear. A sudden imposition of a surface stress in the x direction at $t = 0$ created a turbulent field that deepened with time through the stratified fluid. The "mixed-layer" depth h will be defined here as the depth beyond which the velocity becomes less than 0.2 cm s^{-1}. Fig. 2 shows the variation of h with the nondimensional time $t_i = t/T_i$. The inset in this figure shows the temperature profiles at $t_i = 0.5$ and 3.0, showing the development of a layer well mixed in temperature.

a. *Small times ($t_i < 0.25$)*

Fig. 3 shows the velocity and temperature distributions for $t_i < 0.4$. It is apparent that in the range

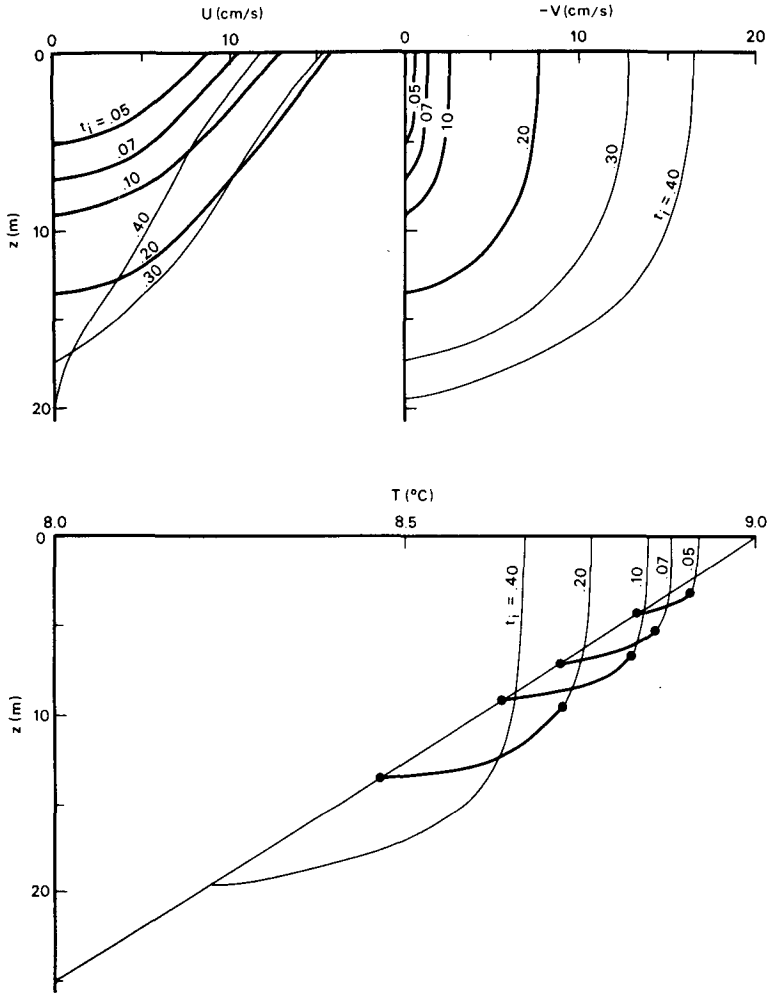

FIG. 3. Development of velocity and temperature profiles for small times. $\tau_0 = 1.5$ dyn cm^{-2}.

$0.05 < t_i < 0.25$, the velocity and temperature profiles are self-similar. The self-similarity breaks down for $t_i < 0.05$ during which the motion starts up from rest, and for $t_i > 0.25$ for which Coriolis forces become important. It is shown in Kundu (1980) that if there is no Coriolis parameter in the problem and a constant critical gradient Richardson number J is imposed at the interface,[1] then self-similarity holds for $100 < tN < 500$. It is shown there that some consequences of self-similarity with initially linear stratification N are that (i) the temperature and velocity gradients at a fixed value of $\eta = -z/h(t)$ are constant in time; (ii) the mixed-layer depth follows the rule $h \approx (4J)^{1/4}u_*(t/N)^{1/2}$; (iii) the depth-average velocity behaves as $\hat{U} \approx (4J)^{-1/4}u_*(tN)^{1/2}$; and (iv) the bulk Richardson number $\hat{\mathrm{Ri}} = gh\Delta\rho/\rho\hat{U}^2$, where $\hat{U}$ is the depth-average velocity and $\Delta\rho$ is the depth-average density difference between the mixed-layer fluid and that just below the interface, remains constant during deepening and is related to the critical gradient Richardson number by

$$\hat{\mathrm{Ri}} \approx 2J. \tag{9}$$

Consequence (i) is evident in Fig. 3, and consequences (ii), (iii) and (iv) were found to be in fair agreement with the present numerical computations.

b. *Sharpening of interface*

It was found that the well-rounded mixed layer bottom of Fig. 3 sharpened into a steep interface for about $t_i > 1$. The sharpening is evident from the inset of Fig. 2, which compares the temperature profiles at $t_i = 0.5$ and 3.0. This sharpening may not, however, be due to the Coriolis forces becoming important. It is shown in Kundu (1980) that the sharp interface appears for $tN > 500$, without

[1] Strictly speaking, the present model does not really have a gradient Richardson number criterion, but a flux Richardson number criterion $R_{f_{cr}} \approx 0.3$ (since $P/\epsilon \approx 1$). But since the gradient and flux Richardson numbers are related by $J = R_f\sigma$, and the turbulent Prandtl number $\sigma(\sim 0.6-1.5)$ does not vary a great deal near the interface, the flux and gradient Richardson number criteria do not give very different results.

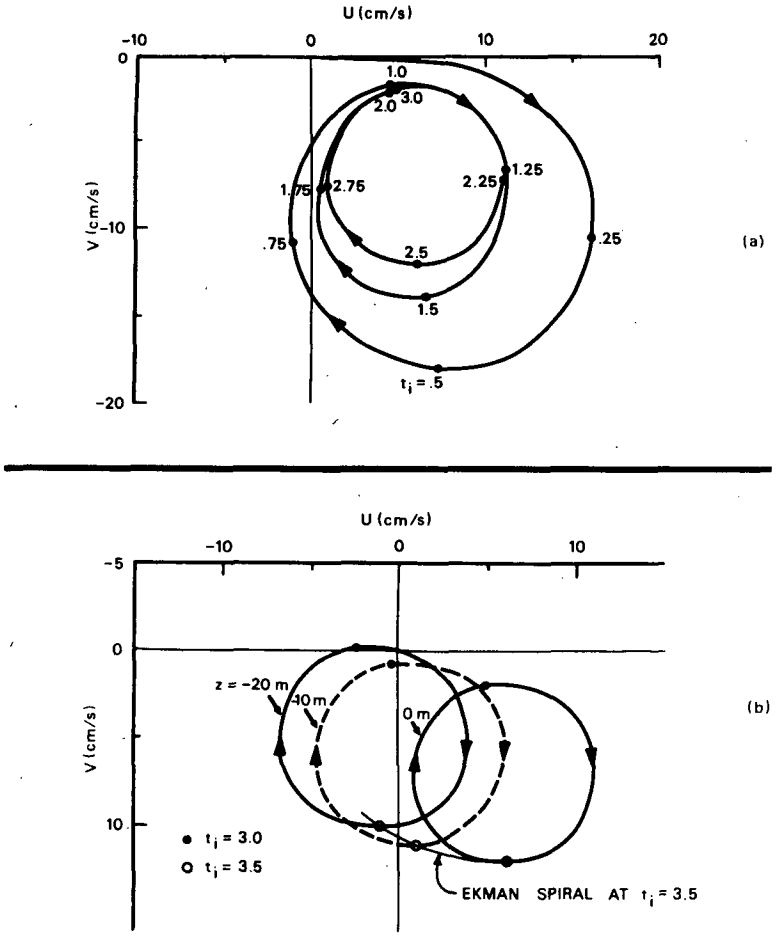

FIG. 4. (a) Hodograph of the surface velocity. The numbers along the path indicate time in inertial periods. (b) Hodographs at depths of $-z = 0$, 10 and 20 m for the inertial period from $t_i = 3$ to $t_i = 4$. Wind stress $\tau_0 = 1.5$ dyn cm^{-2}.

Coriolis forces. With the presently assumed value of $N/f \approx 93.8$, the limit $tN = 500$ corresponds to $t_i \approx 0.85$. The reason for the sharpening is more fully explained by Kundu. Briefly, note that the magnitude of the heat flux $\overline{\theta w}$ must be zero at $z = 0$ and $-h$, and was found to have a maximum at a point (call it M) slightly above the layer bottom. The temperature gradient T_z increases monotonically with depth throughout the mixed layer (Fig. 3). Therefore, below point M, an increase of T_z is associated with a decrease of the heat flux, as if it were a diffusive system with a negative apparent diffusivity. Such a behavior would tend to sharpen an initially diffused profile (Posmentier, 1977).

c. *Velocity field*

The development of the velocity field at various depths is shown in the hodograph plots of Fig. 4. Fig. 4a is the hodograph of the surface velocity, with t_i marked at various points in the path. The hodograph almost repeats itself after about $t_i = 2$, after which the deepening slows down considerably. The initial velocities are larger because the mixed-layer depth is smaller, the depth-integrated velocities being constrained by the relations

$$\int_{-D}^{0} U dz = (\tau_0/f) \sin 2\pi t_i,$$

$$\int_{-D}^{0} V dz = (\tau_0/f)(-1 + \cos 2\pi t_i),$$

where $D > h$. The depth-integrated hodograph is therefore a circle with its center at $(0, -\tau_0/f)$ and radius τ_0/f, which was verified in the solutions. The velocity at a certain depth is zero until the mixed layer reaches it, after which it goes through a transient period and then executes almost periodic (slightly damped) inertial oscillations. These points are nicely illustrated in Mellor and Durbin.

Fig. 4b shows the hodographs at depths of 0, 10 and 20 m for the inertial cycle $3 \leqslant t_i \leqslant 4$. It is evident from the equality of the inertial circles at the

three depths that the velocity field consists of a depth-independent (slab) inertial oscillation of half amplitude of ~6 cm s^{-1}, superimposed on a steady shear flow whose depth integral gives the time-mean Ekman transport. For $t_i < 1$, the shear and inertial oscillation cannot be separated as such; the velocity field can then be described as an inertial oscillation with a shear in it. J. McCreary (private communication) has pointed out that this response is similar to the development of the Ekman layer in a layer of constant depth h with a *zero bottom stress*. The bottom stress is indeed negligible in the present numerical model. It is shown in the Appendix that all components of the inertial oscillation with any shear are smeared out by the eddy viscosity ν_t in a time scale $2h^2/\pi^2\nu_t \approx 1$ h with $h = 20$ m and $\nu_t = 200$ cm^2 s^{-1}. The depth-independent components of the inertial oscillation persist, a result of zero bottom stress. In the present model, however, the development of slablike inertial oscillations take nearly an inertial period, not just one hour; presumably this delay occurs because the mixed-layer depth is not constant, but increases rapidly, for $t_i < 1$.

The time mean flow (U_m, V_m) at later stages, after the inertial oscillations are taken out, is shown in Fig. 5. [The decay of the inertial oscillations would, in the real world, be caused mainly by the radiation of internal waves from the base of the mixed layer (Kundu, 1976)—a process not modeled here.] This is obtained by time-averaging the velocities for one inertial cycle starting at $t_i = 3.0$. The Ekman spiral in depth (Fig. 5b) is not totally unlike that in a constant eddy viscosity model. The surface velocity is at 51° to the right of the wind.

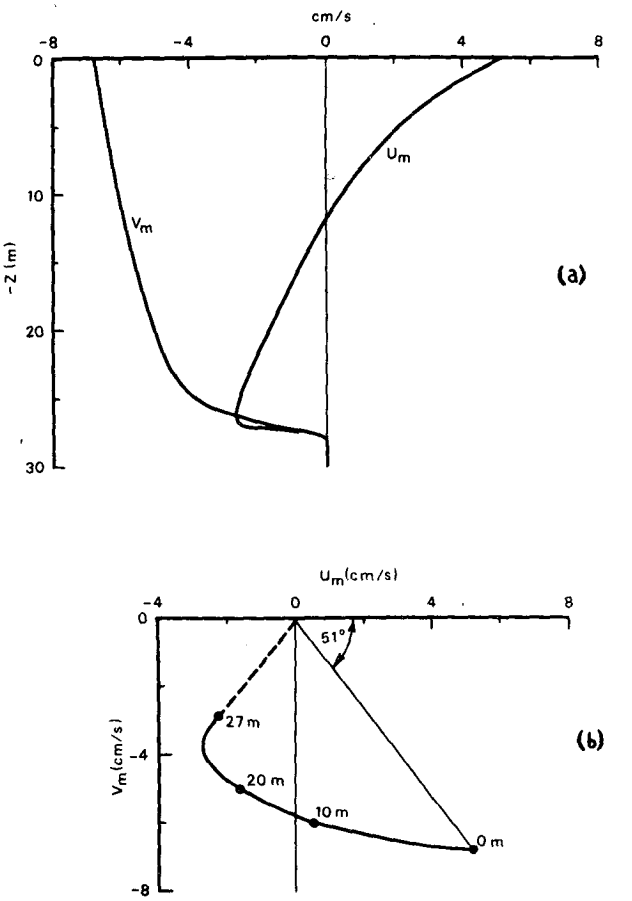

FIG. 5. (a) Quasi-steady velocity profiles, obtained by subtracting the inertial oscillations from $t_i = 3$ to 4. (b) Quasi-steady Ekman spiral. The dashed part is below the turbulent layer. Wind stress $\tau_0 = 1.5$ dyn cm^{-2}.

d. Depth-integrated energetics

The vertically integrated energy balance, obtained by depth-integrating the different terms in Eq. (5), is shown in Fig. 6 as a function of time. For a fixed N/f (=93.8 in the present case), the terms should scale with u_*^3, as was verified by obtaining solutions with $\tau_0 = 1.0$, 1.5 and 2.0 dyn cm^{-2}, and observing that the points indeed lie close to the universal behavior shown. The behavior is similar to that of the Mellor-Durbin model, although less noisy, presumably because of retention of transport terms and use of a smaller time step. The vertical integral of the transport term being zero, the shear production minus the buoyant destruction very nearly balances the viscous dissipation, plus a small difference (~ 0.005–$0.02u_*^3$) equal to the rate of increase of turbulent kinetic energy in the water column, not shown in the figure. The terms increase during the initial stages ($t_i < 0.25$), after which there is a slow decay up to about $t_i = 1.0$. Beyond that, the terms reach a quasi-steady state where the dissipation $\approx 4.4u_*^3$ and shear production $\approx 4.6u_*^3$. Note that the buoyant destruction in the water column, or the rate of increase of potential energy, reaches a maximum of $\sim 1.1u_*^3$. In applications of the Kraus-Turner theory, it is usually assumed that the rate of increase of potential energy due to deepening is ~ 1.0–$1.2u_*^3$, the "wind-wave input" (Kraus and Turner, 1967; Denman, 1973; Niiler, 1975). According to the present model it is nearly u_*^3 for $0.25 < t_i < 0.5$, but smaller outside this range. For about $t_i > 1$, it decays very slowly, from a value of $\sim 0.28u_*^3$ at $t_i = 1.5$ to $\sim 0.23u_*^3$ at $t_i = 4$.

For comparison, the work done by the wind stress is also shown in Fig. 6, which plots one-fifth of $\tau_0 U_0/u_*^3$. As expected from the surface velocity plot of Fig. 4a, the work done is very nearly a sinusoidal function of time, with the maxima at about $t_i = 0.25$, 1.25, 2.25, etc. For initial times ($t_i < 0.25$), both $\tau_0 U_0$ and $\partial(\mathrm{PE})/\partial t$ are increasing functions of time, and an important question is: how much of the work goes into potential energy increase. Fig. 6 gives this as ~8%. This value agrees with the expressions obtained from similarity agruments for small t_i, which give $h \approx (4J)^{1/4}u_*(t/N)^{1/2}$ and $\hat{U} \approx (4J)^{-1/4}u_*(tN)^{1/2}$. The rate of change of potential energy of the water column is approximately

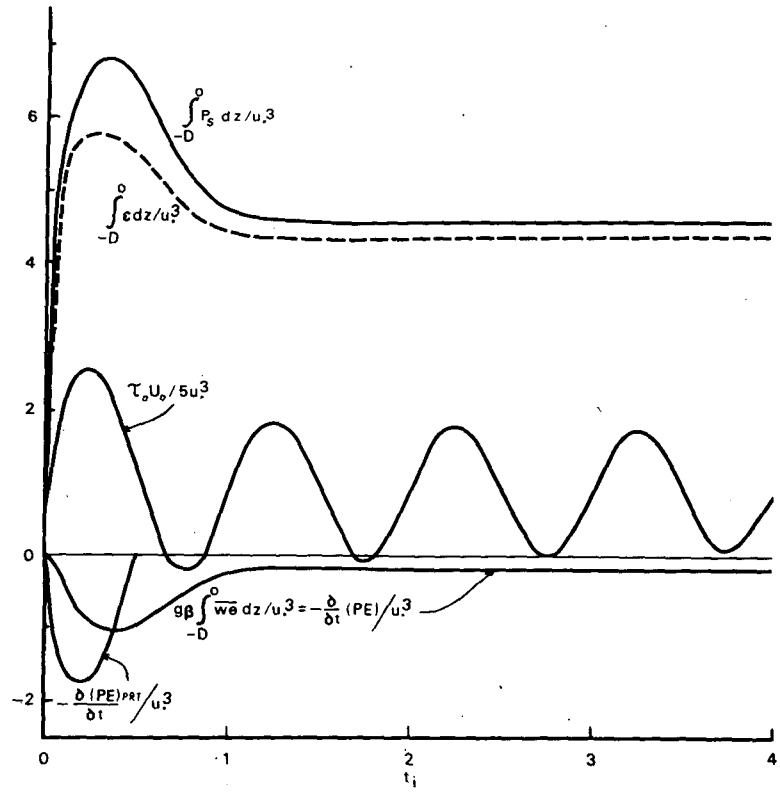

FIG. 6. Depth integrals of shear production P_s, dissipation ϵ, buoyant production $g\beta\overline{w\theta}$ of present and PRT models, and one-fifth of work done by surface wind stress.

$$\dot{PE} \approx \tfrac{1}{4}N^2h^2\frac{dh}{dt}, \tag{10}$$

where the numerical factor of 1/4 on the right-hand side is exact for a slablike density profile (for proof see Kato and Phillips, 1969), and somewhat less for a non-homogeneous density profile. On substitution of the expression for h, Eq. (10) gives $\dot{PE} = \partial(PE)/\partial t \approx \frac{1}{8}(4J)^{3/4}u_*^3(tN)^{1/2}$. Taking the surface velocity to be $\sim 1.5\hat{U}$ (see Fig. 3), the work done by the stress is $W \approx 1.5(4J)^{-1/4}u_*^3(tN)^{1/2}$. This gives the ratio $\dot{PE}/W \approx J/3 \approx 10\%$. Using a numerical factor of 1/5 on the right-hand side of (10) would have made this ratio to be ~8%.

For times $1 < t_i < 4$, $\dot{PE}$ settles to a nearly constant value, and its magnitude should be compared with the average value of $\tau_0 U_0$; i.e., the work done if the inertial oscillations are taken out. Fig. 6 shows that ~5% of this work goes into increase of potential energy after $t_i > 1$.

Also shown in Fig. 6 is the rate of change of potential energy for the PRT model given by

$$\frac{\partial(PE)_{PRT}}{\partial t} = \frac{u_*^3}{4\sqrt{2}}\left(\frac{N}{f}\right)^{1/2}\sin 2\pi t_i(1-\cos 2\pi t_i)^{-1/4}, \quad t_i \leq \tfrac{1}{2}, \tag{11}$$

which reaches maximum at $t_i \approx 0.2$ and goes to zero at $t_i = \frac{1}{2}$. For initial deepening ($t_i < 0.2$), the time variation of the PRT potential energy increase is similar to but larger than that for the present model, as would be expected since the PRT mixed-layer depth is larger than the model h in this region (Fig. 2). (It is also evident that the behavior of the curves in Fig. 6 are universal only in that they are proportional to u_*^3, but each may depend on the ratio N/f. However, no attempt was made to determine how the scales should depend on N and f for the various time ranges.)

To investigate more fully the possible power law behavior of h and $\dot{PE}$ with time, Fig. 7 shows the variation of h and $\dot{PE}$ versus t_i on a log-log plot up to $t_i = 40$. It is evident that in the range of $0.05 < t_i < 0.25$, both $\dot{PE}$ and h behave like $t^{1/2}$, in agreement with the similarity relations or the PRT formulation. The deepening rate slows down after half an inertial period. For $N = 0.94 \times 10^{-2}$ s^{-1}, the potential energy is seen to decrease very slowly in the range $1 < t_i < 6$, somewhat slower than $\dot{PE} \propto t^{-1/4}$, and a deepening rate somewhat faster than $h \propto t^{1/4}$. In fact, a Kraus-Turner type $\dot{PE}$ = constant and $h \propto t^{1/3}$ would not be a bad approximation. These power laws, however, are somewhat tentative because of the considerable noise in the $\dot{PE}$ calculations. For

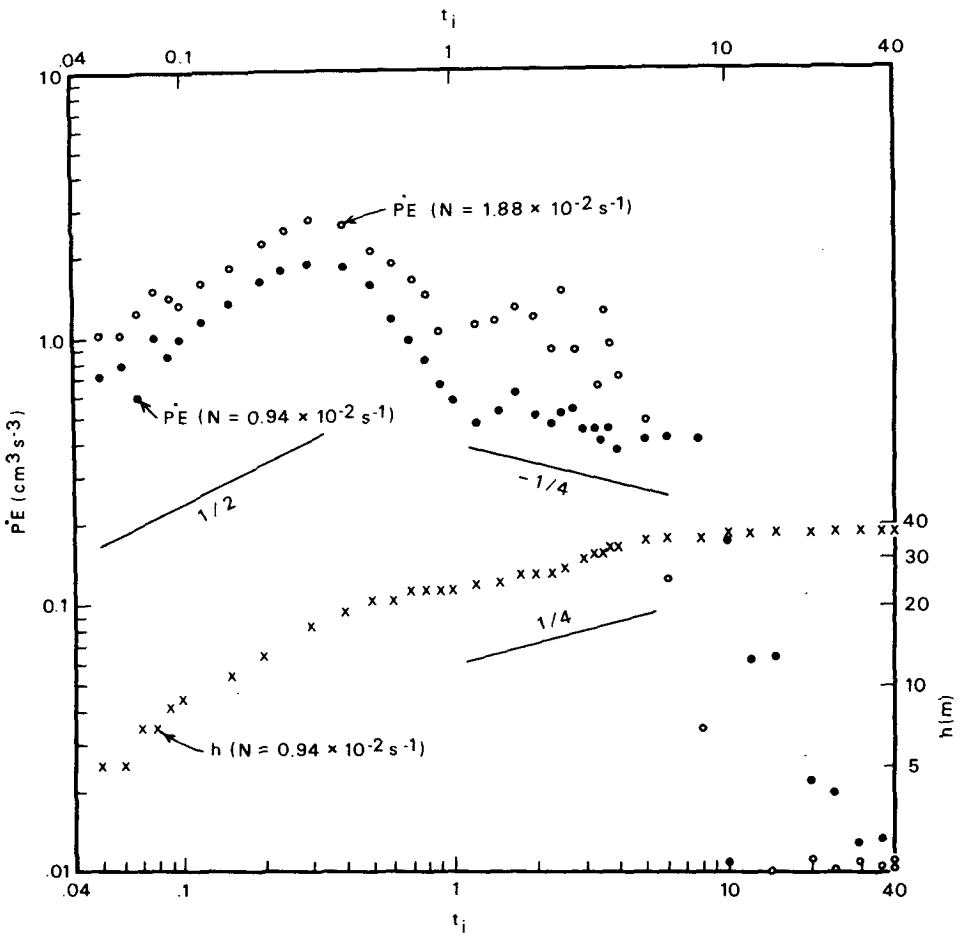

FIG. 7. Log-log plot of the time variations of the mixed-layer depth h (for $N = 0.94 \times 10^{-2}$ s^{-1}) and the rate of change of depth-integrated potential energy $\dot{PE}$ (for $N = 0.94 \times 10^{-2}$ s^{-1} and $N = 1.88 \times 10^{-2}$ s^{-1}).

$t_i > 8$, $\dot{PE}$ decreases very sharply, and no deepening was detected for $t_i > 12$ with a vertical resolution of $\Delta z = 1$ m. Using $N = 1.88 \times 10^{-2}$ s^{-1}, a value twice as large, the layer seemed to stop deepening earlier, at $t_i = 5$ (Fig. 7). The continual deepening up to $t_i = 100$ observed by Mellor and Durbin could be due to their taking a nonuniform $N(z)$, with the stratification decreasing with depth.

e. *Vertical structure*

The energy balance as a function of depth is of interest, especially to see if the turbulent diffusion term is important. Fig. 8 shows the vertical distributions of the terms in the kinetic energy equation (5) for $\tau_0 = 1.5$ dyn cm^{-2} at $t_i = 3.0$. The buoyant destruction term, already included in P, is also shown for comparison. By calculating solutions for $\tau_0 = 1.0$, 1.5 and 2 dyn cm^{-2}, it was again noted that these variables, when plotted as Ph/u_*^3, etc., vs z/h, approximately collapsed into universal distributions for $t_i \geq 2.5$. The numerical values of ϵ in Fig. 8 are in fair agreement with values measured by Stewart and Grant (1962), who report $\epsilon \approx 0.02$ cm^2 s^{-3} for $-z \approx 1$–2 m, and much less for $-z \approx 15$ m.

The turbulent transport term $\partial(\nu_t \partial q^2/\partial z)/\partial z$ is seen to transfer turbulent kinetic energy from near the surface where $P > \epsilon$, to deeper layers where $P < \epsilon$. It is generally smaller than P and ϵ, except in the range 17–22 m where they are comparable. The diffusion is seen to be generally larger than the local rate of change of potential energy $-\beta g \overline{w\theta}$. This does not, however, mean that the diffusion is contributing to the deepening, since near the interface the transport term is negligible. Therefore it does not contribute to deepening, and the idea of Garwood (1977), that this term supplies the kinetic energy near the interface necessary to lift the denser fluid from below, does not agree with the present calculations.

Fig. 9 gives the vertical distributions of the eddy viscosity ν_t, the kinetic energy flux $\nu_t \partial q^2/\partial z$, and a turbulence length scale defined by $l = q^3/5.3\epsilon$, for $t_i = 3$ and $\tau_0 = 1.5$ dyn cm^{-2}. Fig. 10 shows the vertical distributions of the corresponding stresses

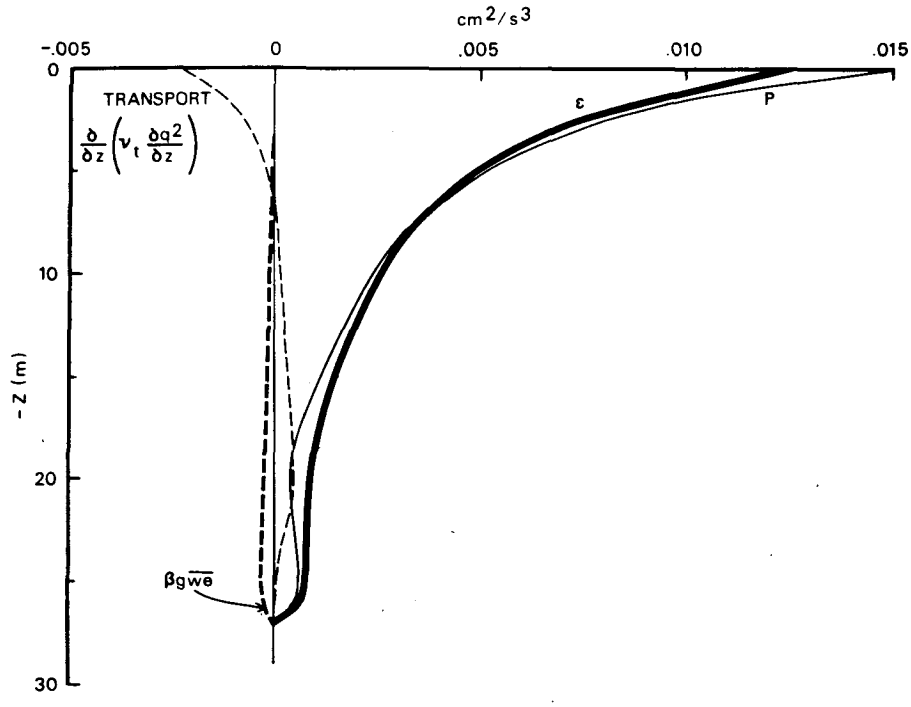

FIG. 8. Vertical profiles of the turbulent kinetic energy budget at $t_i = 3$. P is the *net* production (shear production minus buoyant destruction). Wind stress $\tau_0 = 1.5$ dyn cm^{-2}.

and kinetic energy. Note that although the turbulence intensity q^2 is maximum at the sea surface, ν_t is maximum well inside the interior. This is because $\nu_t \propto q^4/\epsilon$, and ϵ increases faster than q^4 as $|z| \to 0$. The behavior of the eddy viscosity is somewhat similar to that in Worthem and Mellor (1980), who choose $l = -\kappa z$ near the sea surface[2] (κ is the von Karman constant) and hence obtain a ν_t distribution that goes to zero at $z = 0$. The surface eddy viscosity in the present model is about half the maximum value.

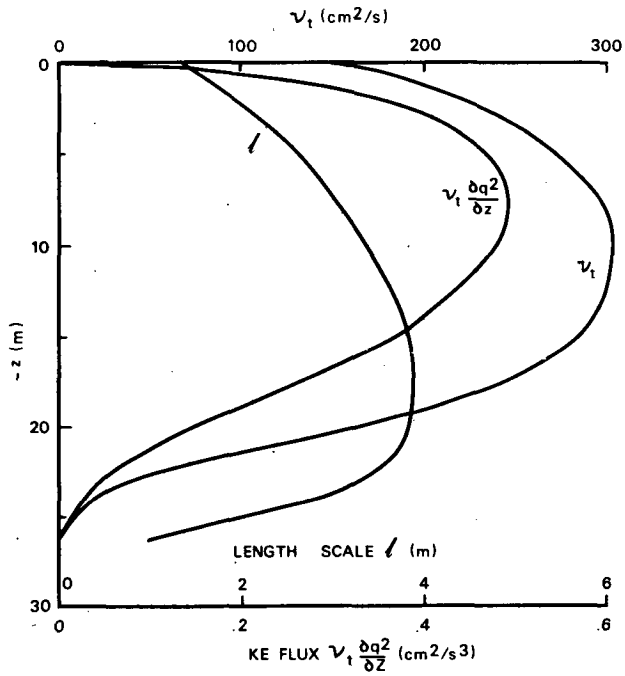

FIG. 9. Vertical profiles of the eddy viscosity, kinetic energy flux and the turbulence length scale. Wind stress $\tau_0 = 1.5$ dyn cm^{-2}.

In the absence of waves, the eddy coefficient may indeed be maximum in the middle. In the laboratory experiment of Kato and Phillips (1969), for example, the mean velocity has been described to vary most rapidly near the driving screen and the entrainment interface, and almost uniform in the central region. This would seem to imply an eddy coefficient lower near the surface than in the middle.

The consistency between the stress distributions in Fig. 10 and the velocity distributions in Fig. 5 could be checked by splitting the solution into a quasi-steady mean shear and a depth-independent inertial oscillation. That is, $U = U_m + U_i$, $V = V_m + V_i$, where approximately

$$\left.\begin{aligned} \frac{\partial U_i}{\partial t} - fV_i = 0, \quad \frac{\partial V_i}{\partial t} + fU_i = 0 \\ -fV_m = \frac{\partial}{\partial z}(-\overline{uw}) \quad fU_m = \frac{\partial}{\partial z}(-\overline{vw}) \end{aligned}\right\}.$$

[2] This choice does not seem to be easy to defend. Such a rigid-lid assumption would be appropriate in the atmospheric case, but not in the oceanic case.

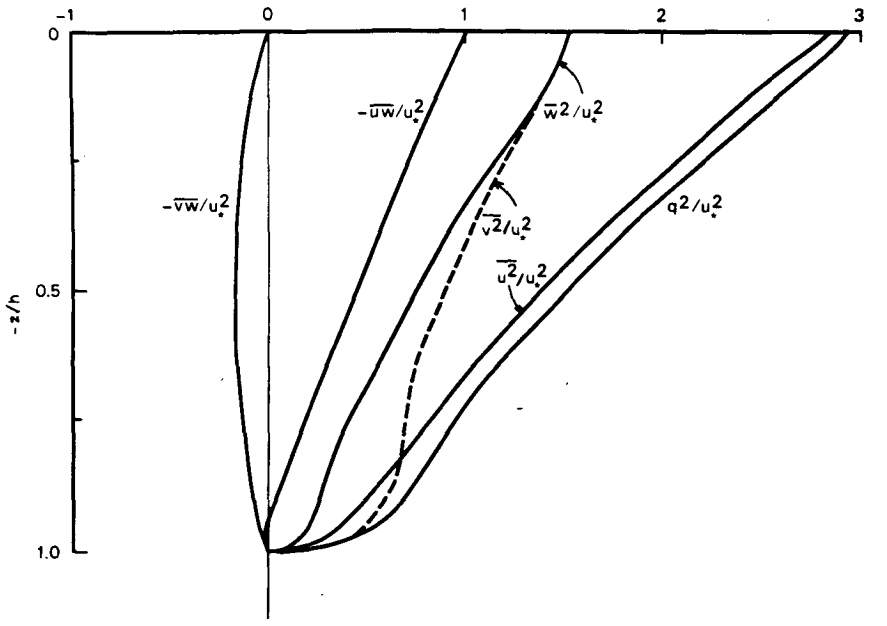

FIG. 10. Vertical profiles of stresses and kinetic energy.

The uniform curvature of the $\overline{vw}$ profile gives rise to the uniform shear in U_m. The small shear of V_m in the top 80% of the mixed layer, and the large shear of V_m in the bottom 20%, are consistent with the small curvature of $\overline{uw}$ in the top part and the larger curvature of $\overline{uw}$ in the bottom part. These facts were verified by using actual numerical values and finding agreement with the above equations.

4. Comparison with PRT

PRT assume that the eddy coefficients in the mixed layer are so large that the velocity and density profiles are slablike. The deepening rate is specified by the criterion that

$$\hat{\mathrm{Ri}} = \frac{gh\Delta\rho}{\rho(\hat{U}^2 + \hat{V}^2)} = \text{constant during deepening}, \qquad (12)$$

where the caret denotes the depth-independent PRT variables; $(\hat{U},\hat{V})$ and $\Delta\rho$ are the discontinuities in the velocity and density at the bottom of the layer. PRT originally set $\hat{\mathrm{Ri}} = 1$. Laboratory data (Price, 1979a; Thompson, 1979), field data (Price *et al.*, 1978; Price 1979b), as well as previous numerical solutions (Mellor and Durbin, 1975) show that the PRT theory gives answers of the right order if $\hat{\mathrm{Ri}}$ is set to a somewhat smaller value of the constant, in the range 0.35–0.8.

Neglecting rotational effects ($t_i < 0.25$) and assuming self-similarity but not slablike profiles, Kundu (1980) has shown that $\hat{\mathrm{Ri}} \approx 2J$ = constant during deepening, where in the definition of $\hat{\mathrm{Ri}}$ one identifies $\hat{U}$ with the depth-*average* velocity and $\Delta\rho$ with the depth-average density difference. The relation $\hat{\mathrm{Ri}} \approx 2J$ is in fair agreement with Mellor and Durbin's finding that $\hat{\mathrm{Ri}} \approx 0.35$ with $J = 0.23$. In the present numerical calculations, note from Fig. 2 that $h/h_{\mathrm{PRT}} \approx 0.8$–$0.9$. Since $h_{\mathrm{PRT}} \propto \hat{\mathrm{Ri}}^{1/4}$, it is apparent that setting $\hat{\mathrm{Ri}} \approx 0.6$ would give fair agreement between the present calculations and the PRT theory. The relation $\hat{\mathrm{Ri}} \approx 2J$, therefore, seems valid.

The bulk and gradient Richardson number criteria are therefore equivalent, a consequence of self-similarity. If δ is the thickness of the "interface" within which the local Richardson number is nearly equal to the critical value, then the self-similarity would require that the ratio δ/h remains constant during deepening, a result also predicted by Garwood (1977). The heavier lines in Fig. 3 indicate the "interface thickness," defined arbitrarily as the region where the local Richardson number is within 30% of the critical value. It is apparent that the interface thickens, and δ/h does remain constant, for $t_i < 0.25$.

Additional insight into the PRT Richardson number criterion may be obtained by examining the energetics. Substitution of the criterion (12) into the depth-integrated equations of motion gives

$$\tau_0 \cdot \hat{\mathrm{U}} = \frac{\partial}{\partial t}(\hat{\mathrm{KE}}) + \hat{\mathrm{Ri}}^{-1}\frac{\partial}{\partial t}(\mathrm{PE}), \qquad (13)$$

where

$$\hat{\mathrm{KE}} = 1/2\int_{-D}^{0}(\hat{U}^2 + \hat{V}^2)dz,$$

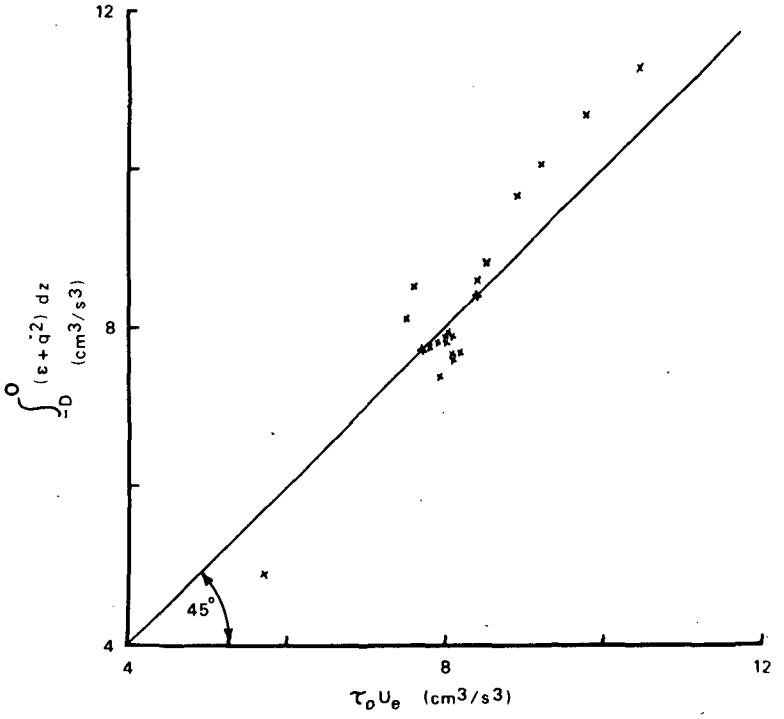

FIG. 11. Verification of Eq. (17). Wind stress $\tau_0 = 1.5$ dyn cm^{-2}.

and $\boldsymbol{\tau}_0 \cdot \hat{\mathbf{U}}$ is the rate of working by the wind on the depth-averaged velocity $\hat{\mathbf{U}}$.

Neglecting viscous transports and the viscous dissipation of the mean kinetic energy, the kinetic energy equations for the mean and turbulent fields are

$$\frac{1}{2}\frac{\partial}{\partial t}(U^2 + V^2) = -\frac{\partial}{\partial z}(\overline{uw}U + \overline{vw}V) - P_s, \quad (14)$$

$$\frac{\partial q^2}{\partial t} = -\frac{\partial}{\partial z}(\overline{wq^2}) + P_s + \beta g \overline{w\theta} - \epsilon, \quad (15)$$

where P_s is the shear production. Elimination of P_s between (14) and (15), a vertical integration, and an assumption of no flux of q^2 at the surface, give

$$\boldsymbol{\tau}_0 \cdot \mathbf{U}_0 = \frac{\partial}{\partial t}(\mathrm{KE}) + \frac{\partial}{\partial t}(\mathrm{PE}) + E, \quad (16)$$

where $\mathbf{U}_0$ is the surface velocity,

$$\partial(\mathrm{PE})/\partial t = -\beta g \int_{-D}^{0} \overline{w\theta} dz,$$

and

$$E = \int_{-D}^{0} (\epsilon + \partial q^2/\partial t) dz$$

is nearly the total dissipation in the water column (since $\partial q^2/\partial t \ll \epsilon$). The present model calculations, of course, obey (16). Due to the presence of the shear, however, the surface velocity $\mathbf{U}_0$ will be larger in magnitude than the depth-averaged velocity $\hat{\mathbf{U}}$, say $\mathbf{U}_0 = \hat{\mathbf{U}} + \mathbf{U}_e$. Assuming that $\partial(\hat{\mathrm{KE}})/\partial t$ can be approximately replaced by $\partial(\mathrm{KE})/\partial t$, note that (13) and (16) will be identical if

$$\frac{\boldsymbol{\tau}_0 \cdot \mathbf{U}_e - E}{\mathrm{PE}} = 1 - \frac{1}{\hat{\mathrm{Ri}}}. \quad (17)$$

Setting $\hat{\mathrm{Ri}} = 1$, as was originally done by PRT, is equivalent to assuming that the "extra work" $\boldsymbol{\tau}_0 \cdot \mathbf{U}_e$ exactly balances the total dissipation in the water column.

All terms on the left side of (17) were evaluated in the present model as a function of time, the depth-average velocity being subtracted from the surface velocity for evaluating $\boldsymbol{\tau}_0 \cdot \mathbf{U}_e$. It was found that $\boldsymbol{\tau}_0 \cdot \mathbf{U}_e$ and E are indeed of the same order for all times (Fig. 11). This, however, does not mean that $\hat{\mathrm{Ri}}$ is nearly 1 for all times, since PE in (17) is an order of magnitude smaller than $\boldsymbol{\tau}_0 \cdot \mathbf{U}_e$ and E, and one is dealing here with the small difference between two large numbers. It was found that $(\boldsymbol{\tau}_0 \cdot \mathbf{U}_e - E) < 0$ for $t_i < 0.5$, and $(\boldsymbol{\tau}_0 \cdot \mathbf{U}_e - E) > 0$ for $t_i > 1$. This is consistent with (17), since $\hat{\mathrm{Ri}} \approx 0.6$ for $t_i < 0.5$, and $\hat{\mathrm{Ri}}$ is presumably a number >1 for $t_i > 1$ during which there is no PRT-type deepening.

It is easy to see why $\boldsymbol{\tau}_0 \cdot \mathbf{U}_e$ should be of the same order as E for all times. For small times $\boldsymbol{\tau}_0 \cdot \mathbf{U}_e$ is nearly half the total surface stress work, and is therefore of the order of E (Fig. 6). For large times ($t_i > 1$),

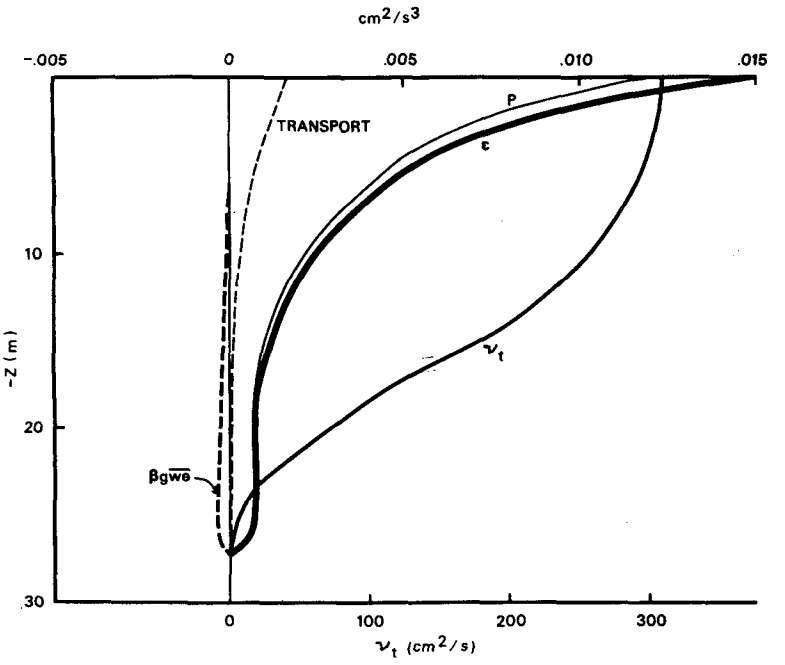

FIG. 12. Vertical profiles of the turbulent kinetic energy budget with surface wave flux, and the distribution of eddy viscosity. P is the *net* production (shear production minus buoyant destruction). Wind stress $\tau_0 = 1.5$ dyn cm^{-2}.

U_e is identical to U_{m0}, the surface value of the time mean profile U_m in Fig. 5. However, $\tau_0 U_{m0}$ is also the average work done in an inertial cycle, and therefore equals E + PE. Eq. (17) shows that $\hat{\text{Ri}}$ must therefore be large in this time range.

5. Solution with wave flux

Some preliminary results have been obtained where a kinetic energy flux has been imposed on the top surface, by means of the boundary condition $\nu_t \partial q^2/\partial z = m u_*^3$ at $z = 0$ on Eq. (5). The energy budget for $m = 0.5$ and $\tau_0 = 1.5$ dyn cm^{-2} is shown in Fig. 12. The transport term is seen to be everywhere positive, and the production near the surface decreases compared to the case with $m = 0$. The effect of the transport term is again negligible near the interface. In fact, the deepening rate is only slightly larger than that with no wave flux.

The interesting change from the previous solution is that the eddy viscosity is no longer maximum in the middle (Fig. 12), which is due to the fact that q^2 is now higher near the surface. This is a desirable feature in the solution, since all the observations summarized in the review paper by Pollard (1977) show that the eddy coefficients are largest (~200–400 cm^2 s^{-1}) near the sea surface. The increase of ν_t near the surface only decreases the velocity gradients near the surface, but otherwise the dynamics was found to remain essentially unchanged from the case with no surface wave flux. For example, the depth-integrated energy balance was very similar to Fig. 6.

6. Summary and discussion

The structure of the turbulent stratified upper mixed layer of the ocean has been numerically investigated by applying the turbulence closure model of Gibson and Launder. The model retains the turbulent diffusion terms and involves the solution of differential equations for q^2 and ϵ and algebraic equations for the stresses and heat fluxes. Solutions have been obtained under the action of an impulsive wind stress and a zero surface heat flux.

Most of the solutions described here have a zero surface kinetic energy flux. The resulting mean motion consists of depth-independent inertial oscillations superimposed on a time-mean shear which somewhat resembles an Ekman spiral with a surface velocity of 51° to the right of the wind. There is evidence [Fig. 14 of Halpern (1976); Fig. 8 of Kundu (1977)] that sub-inertial-scale motion in the surface layer is sometimes indeed very much like an Ekman spiral with surface veering of order 30–45°.

The turbulent diffusion term is in general smaller than P or ϵ, but comparable to $-\beta g \overline{w\theta}$. It transfers energy downward from near the surface, but its contribution to deepening is negligible. The negligible values of diffusion near the base result from the small local magnitude of ν_t. This conclusion would therefore not hold if the gradient diffusion law used

here were found to be totally inadequate in the ocean. The retention of the diffusive terms has the merit, however, of avoiding jittery solutions, and the present solutions were smoother than Mellor and Durbin's. In fact, instabilities were found to result in the present model if the diffusive term in either the q^2 or the ϵ equation was dropped.

The present work does not, however, conclusively demonstrate that turbulent diffusion is unimportant in oceanic mixed layers. First, the convective situation resulting from a surface heat loss has not been considered. Second, all closure models derive the values of their principal constants from laboratory experiments. But oceanic turbulence might very well be different from laboratory turbulence. The patchiness of ocean turbulence, Langmuir circulations, etc., do not have their laboratory counterparts, and the assertion that turbulence is universal may not include the oceanic situation. Third, the model fails in the absence of any shear. But the interface does propagate in the stirring experiments of Turner (1968) in which there is no shear, certainly due to turbulent diffusion. Although it is quite unlikely that this mechanism would be effective during the initial rapid deepening period, such a "stirring" mechanism could possibly simulate processes on the seasonal time scales.

The time variation of the rate of increase of potential energy in the water column (Fig. 6) shows several interesting features. For $0.05 < t_i < 0.3$, it is seen that PE varies like $t^{1/2}$, reaching a maximum of $\sim 1.1 u_*^3$ at $t_i \approx 0.3$. (The maximum value would, of course, depend on N and f. The value of $1.1 u_*^3$ is valid only for the assumed values of $N = 0.94 \times 10^{-2}$ s^{-1} and $f = 10^{-4}$ s^{-1}.) PE for the PRT model also varies like $t^{1/2}$ for small times, although its magnitude is about twice as large, implying that the critical Richardson number in the PRT model should be set to ~ 0.6 for the equivalence of the two model calculations. With the left-hand side of (10) varying like $t^{1/2}$, an integration gives $h \propto t^{1/2}$ as in the PRT deepening for small times.

For $1 < t_i < 6$, PE decays only slightly from a quasi-steady value of $\sim 0.25 u_*^3$, implying a deepening rate slightly smaller than the Kraus-Turner $h \propto t^{1/3}$, possibly about $h \propto t^{1/4}$. The reason why PE settles down to a nearly constant value for $t_i > 1$ is because the motion then separates into a depth-independent inertial oscillation and a quasi-steady shearing motion. All the turbulent stresses are carried by the shearing motion, except a small stress at the bottom of the inertial slab. The turbulent field therefore reaches a quasi-steady state, and the vertical distributions of P, ϵ, $\overline{uw}$, $\overline{w\theta}$, etc., do not vary much with time. Hence, $\beta g \int \overline{w\theta} dz$ reaches a nearly constant value.

A comparison of the PE and $\tau_0 U_0$ variations in Fig. 6 shows that during initial deepening ($t_i < 0.25$), about 8% of the work goes into potential energy increase, whereas for large times ($t_i > 1$), about 5% of the average work during an inertial cycle goes to PE.

Although the deepening rate is not far from $h \propto t^{1/3}$ for large times, the *mechanism* is not as implied in Kraus and Turner. They did not explicitly talk of the importance of the turbulent diffusion term, but their idea of the wave-generated turbulence being used for deepening implies turbulence diffusion. In the absence of significant transport to the base of the mixed layer, the mechanism of deepening in the present model is the local production (or equivalently, local shear) at the base. The shear of both the mean and the inertial oscillation at the layer base must contribute to this deepening, and there are several pieces of evidence for this fact. First, slight inertial oscillations were evident in the magnitude of the shear production P_s near the base; P_s reaches maxima near about $t_i = 1.7, 2.7$, etc., at which times the shear of the quasi-steady motion and the inertial oscillation are in the same direction at the layer base. Second, the slow decay of the inertial oscillations (e.g., in the $\tau_0 U_0$ curve in Fig. 6) must be due to the production of turbulence at its base. The decay is not viscous, since virtually the same decay rate was observed by setting molecular viscosity to zero in the calculations.

If the inertial production near the layer base does make a contribution, then one wonders why there is no inertial oscillation in PE in Fig. 6 for large times. The reason is, because of the absence of inertial shear elsewhere, the oscillations in P_s and $\overline{w\theta}$ occur only near the layer base. When integrated over the depth, these small oscillations do not stand out. If the inertial currents were taken out, PE is not expected to settle down to a value much smaller than $0.25 u_*^3$, because they do not contribute to any smearing of the heat throughout the layer.

For $t_i > 12$ if $N = 0.94 \times 10^{-2}$ s^{-1}, and for $t_i > 5$ if N is twice as large, PE dropped sharply and no deepening was detected with a vertical resolution of $\Delta z = 1$ m. It was expected that the layer would probably finally stop deepening because, in view of the Appendix, the shear (velocity jump) at the layer base would decrease when h becomes much larger than the Ekman depth. No appreciable decrease of shear at the layer base was detected, however, probably because the mixed layer depth was never an order of magnitude larger than the Ekman depth. The reason for the rather sudden and sharp drop of PE, and the accompanying cessation of deepening, is not therefore very clear. The question, however, is merely academic as far as the application to the real ocean is concerned, since the wind stress would hardly remain constant for more than 12 inertial periods!

The assumption necessary to derive the PRT

energy equation for mean flow, namely, that the depth-integrated dissipation approximately balances $\tau_0 \cdot (\mathbf{U}_0 - \bar{\mathbf{U}})$, has been shown to be a reasonable one. The model results also suggest that the bulk Richardson number criterion of PRT is equivalent to a constant critical gradient Richardson number at the base of the mixed layer. This has been observed to result from a self-similarity of the solutions, giving rise to a thickening of the interface during initial ($t_i < 0.5$) deepening.

An imposition of a kinetic energy flux at the sea surface, so as to simulate the energy input due to breaking waves, has been shown to give an eddy viscosity profile that is maximum near the sea surface. However, the detailed structure of the eddy viscosity does not seem to affect the results very much. No vertical profile of ν_t was given by Mellor and Durbin, but our duplication of their model calculation with a constant wind stress and zero heat flux showed that their ν_t was maximum at the surface. The behavior of ν_t in the present model without wave flux was different (Fig. 9), yet the structure and dynamics of the mean and turbulent fields are similar to theirs. It seems that the various second-order closure models would give results that may differ in details, like the distributions of Prandtl number, ratios of normal stresses, even eddy viscosity, etc. However, at least the depth-integrated dynamics (Fig. 6), which is of prime interest for mixed layer calculations, would not be different. There is something basic about the dynamics that is obeyed by all the numerical schemes, and hopefully the real world. For small times ($t_i < 0.25$), this basic fact seems to be self-similarity (Kundu, 1980), and for large times ($t_i > 1$), it is the separation of the flow into a steady shear and a depth-independent inertial oscillation.

Two important aspects have been left out of the present calculations. One is the effect of surface heating and cooling, and the other is the determination of the vertical distributions of temperature variance, temperature dissipation, etc., which are presently being measured in the ocean. These will be dealt with in a future work.

APPENDIX

Currents in a Layer of Constant Depth and No Bottom Stress

The development of currents in a mixed layer of *constant depth* h and uniform viscosity ν_t under the action of an impulsive surface stress τ_0 in the x direction is presented here. The assumptions of a depth h less than the Ekman depth $(2\nu_t/f)^{1/2}$ and a *zero bottom stress* cause the velocity to approach the bottom with a finite value and zero slope, somewhat like Fig. 5a.

Defining a complex velocity $W = U + iV$, the equation to be solved is

$$\frac{\partial W}{\partial t} + ifW = \nu_t \frac{\partial^2 W}{\partial z^2},$$

with boundary and initial conditions $\partial W/\partial z = \tau_0/\rho\nu_t$ at $z = 0$; $\partial W/\partial z = 0$ at $z = -h$; and $W = 0$ at $t = 0$. The solution is (Nomitsu, 1933)

$$W = \frac{(1-i)\tau_0 \cosh(1+i)k(h+z)}{2\rho\nu_t k \sinh(1+i)kh} + \frac{i\tau_0}{\rho\nu_t k^2 h} e^{-ift}\left[\frac{1}{2} + \sum_{n=1}^{\infty} \frac{1 + \frac{1}{2}i(\beta_n/k)^2}{1 + \frac{1}{4}(\beta_n/k)^4} \times \cos\beta_n z \exp(-\nu_t \beta_n^2 t)\right],$$

where $k = (f/2\nu_t)^{1/2}$ and $\beta_n = n\pi/h$. The first part in the solution is the steady component, and is similar to an Ekman spiral with a finite bottom velocity, much like Fig. 5. The second part of the solution, which is needed to satisfy the initial condition of no motion, is composed of inertial oscillations. The depth-independent component of this persists undamped, while those with shear are damped within a time $t_d \approx 2/\nu_t\beta_1^2 = 2h^2/\pi^2\nu_t$. The values appropriate for the present numerical model are $h \approx 20$ m and $\nu_t \approx 200$ cm^2 s^{-1}, giving $t_d \approx 1$ h.

Note that in the classical Ekman solution with no slip condition at the bottom, the depth-independent component of the inertial oscillation is not possible, and all components of the inertial oscillations decay. The possibility of an undamped depth-independent inertial oscillation is solely a result of a "slippery bottom."

It can also be verified from the solution given that the shallower the depth h with respect to the Ekman depth k^{-1}, the greater the deviation α of the steady surface current from the direction of the wind. The veering $\alpha \approx 45°$ if $h \gg k^{-1}$, and $\alpha \approx 90°$ if $h \ll k^{-1}$. This makes sense, since the steady velocity is almost uniform across the layer if $h \ll k^{-1}$. In the present numerical solution $\alpha \approx 51°$.

Acknowledgments. I am grateful to Dr. McCreary for many fruitful discussions and comments on the manuscript. Comments on the manuscript were also kindly given by Drs. R. Garwood, B. E. Launder, G. L. Mellor, P. P. Niiler, J. F. Price and R. O. R. Y. Thompson. The work was supported by the National Science Foundation under Contract OCE-7819703.

REFERENCES

Denman, K. L., 1973: A time-dependent model of the upper ocean. *J. Phys. Oceanogr.*, **3**, 173–184.

——, and M. Miyake, 1973: Upper layer modification at ocean station Papa: Observations and simulation. *J. Phys. Oceanogr.*, **3**, 185–196.

de Szoeke, R. A., and P. B. Rhines, 1976: Asymptotic regimes in mixed layer deepening. *J. Mar. Res.*, **34**, 111–116.

Garwood, R. W., 1977: An ocean mixed layer model capable of simulating cyclic states. *J. Phys. Oceanogr.*, **7**, 455–468.

Gibson, M. M., and B. E. Launder, 1976: On the calculation of horizontal, turbulent, free shear flows under gravitational influence. *ASME J. Heat Transfer*, **98C**, 81–87.

Gonella, J., 1970: Le courant de derive d'aprés les observations effectuées á la Bouée Laboratoire. Mus. Nat. d'Hist. Naturalle (unpublished manuscript).

Halpern, D., 1976: Structure of coastal upwelling event observed off Oregon during July 1973. *Deep-Sea Res.*, **23**, 495–508.

Hanjalic, K., and B. E. Launder, 1972: A Reynolds stress model of turbulence and its application to thin shear flows. *J. Fluid Mech.*, **52**, 609–638.

Kato, H., and O. M. Phillips, 1969: On the penetration of a turbulent layer into stratified fluid. *J. Fluid Mech.*, **37**, 643–655.

Kraus, E. B., 1972: *Atmosphere-Ocean Interaction*. Oxford University Press, 275 pp.

——, and J. S. Turner, 1967: A one-dimensional model of the seasonal thermocline: II. The general theory and its consequences. *Tellus*, **19**, 98–106.

Kundu, P. K., 1976: An analysis of inertial oscillations observed near Oregon coast. *J. Phys. Oceanogr.*, **6**, 879–893.

——, 1977: On the importance of friction in two typical continental waters: Off Oregon and Spanish Sahara. *Bottom Turbulence*, J. C. J. Nihoul, Ed., Elsevier, 187–207.

——, 1980: Consequences of self-similarity in entrainment experiments. Submitted to *J. Fluid Mech.*

Launder, B. E., 1975: On the effects of a gravitational field on the turbulent transport of heat and momentum. *J. Fluid Mech.*, **67**, 569–581.

Mellor, G. L., and P. A. Durbin, 1975: The structure and dynamics of the ocean surface mixed layer. *J. Phys. Oceanogr.*, **5**, 718–728.

Niiler, P. P., 1975: Deepening of the wind-mixed layer. *J. Mar. Res.*, **33**, 405–422.

——, and E. B. Kraus, 1977: One-dimensional models of the upper ocean. *Modeling and Prediction of the Upper Layers of the Ocean*, E. B. Kraus, Ed., Pergamon Press, 143–172.

Nomitsu, T., 1933: A theory of the rising stage of drift current in the ocean (I and II). *Mem. Coll. Sci., Kyoto*, **16**, No. 2.

Phillips, O. M., 1977: *The Dynamics of the Upper Ocean*, 2nd ed. Cambridge University Press, 336 pp.

Pollard, R. T., 1977: Observations and models of the structure of the upper ocean. *Modeling and Prediction of the Upper Layers of the Ocean*, E. B. Kraus, Ed., Pergamon Press, 102–117.

——, P. B. Rhines and R. O. R. Y. Thompson, 1973: The deepening of the wind-mixed layer. *Geophys. Fluid Dyn.*, **3**, 381–404.

Posmentier, E. S., 1977: The generation of salinity finestructure by vertical diffusion. *J. Phys. Oceanogr.*, **7**, 298–300.

Price, J. F., 1979a: On the scaling of stress-driven entrainment experiments. *J. Fluid Mech.*, **90**, 509–529.

——, 1979b: Observations of a rain-formed mixed layer. *J. Phys. Oceanogr.*, **9**, 643–649.

——, C. N. K. Mooers and J. C. van Leer, 1978: Observation and simulation of storm-induced mixed layer deepening. *J. Phys. Oceanogr.*, **8**, 582–599.

Rodi, W., 1972: The prediction of free turbulent boundary layers by use of a two-equation model of turbulence. Ph.D. thesis, University of London.

Stewart, R. W., and H. L. Grant, 1962: Determination of the rate of dissipation of turbulent energy near the sea surface in the presence of waves. *J. Geophys. Res.*, **67**, 3177–3180.

Tennekes, H., 1973: A model for the dynamics of the inversion above a convective boundary layer. *J. Atmos. Sci.*, **30**, 558–567.

Thompson, R. O. R. Y., 1979: A re-examination of the entrainment process in some laboratory flows. *Dyn. Atmos. Oceans* (in press).

Turner, J. S., 1968: The influence of molecular diffusivity on turbulent entrainment across a density interface. *J. Fluid Mech.*, **33**, 639–656.

Worthem, S., and G. Mellor, 1980: Turbulence closure model applied to the upper tropical ocean. *Deep-Sea Res.* (in press).

Wyngaard, J. C., O. R. Coté and K. S. Rao, 1974: Modeling of the atmospheric boundary layer. *Advances in Geophysics*, Vol. 18A, 193–211.

Zeman, O., and J. L. Lumley, 1976: Modeling buoyancy driven mixed layers. *J. Atmos. Sci.*, **33**, 1974–1988.